eNeuro Accepted Manuscript

eNeuro

Research Article: Confirmation | Cognition and Behavior

Viral tracing confirms paranigral ventral tegmental area dopaminergic inputs to the interpeduncular nucleus where dopamine release encodes motivated exploration

https://doi.org/10.1523/ENEURO.0282-22.2022

Cite as: eNeuro 2023; 10.1523/ENEURO.0282-22.2022

Received: 12 July 2022
Revised: 7 December 2022
Accepted: 20 December 2022

This Early Release article has been peer-reviewed and accepted, but has not been through the composition and copyediting processes. The final version may differ slightly in style or formatting and will contain links to any extended data.

Alerts: Sign up at www.eneuro.org/alerts to receive customized email alerts when the fully formatted version of this article is published.

Copyright © 2023 Molas et al.
This is an open-access article distributed under the terms of the Creative Commons Attribution 4.0 International license, which permits unrestricted use, distribution and reproduction in any medium provided that the original work is properly attributed.

eNeuro Accepted Manuscript

1
2 **Viral tracing confirms paranigral ventral tegmental area dopaminergic inputs to the**
3 **interpeduncular nucleus where dopamine release encodes motivated exploration**
4
5 **Interpeduncular nucleus dopamine release in motivated exploration**
6
7 Susanna Molas*[1], Rubing Zhao-Shea*[1], Timothy G Freels and Andrew R. Tapper[1]
8
9 [1]Department of Neurobiology, Brudnick Neuropsychiatric Research Institute
10 University of Massachusetts Medical School
11 364 Plantation St, LRB, Worcester, 01605, MA
12
13 SM and RZS performed research. SM, RZS, TGF and ART designed research, analyzed data, and wrote
14 the paper.
15
16
17 **Corresponding author:**
18 **Andrew R. Tapper PhD**
19 **Brudnick Neuropsychiatric Research Institute, Department of Neurobiology, University of**
20 **Massachusetts Medical School, Worcester, MA, 01605, USA.**
21 **Phone: (774)-455-4293**
22 **Email: andrew.tapper@umassmed.edu**
23
24 Number of figures: 5
25 Number of words
26 - Abstract: 250 words
27 - Introduction: 685 words
28 - Discussion: 1418 words

29 **Acknowledgments**
30 We thank Kensuke Futai, Ph.D. for sharing antibody reagents, Leeyup Chung, Ph.D. for insightful input
31 on the experimental design and Biorender.com for use of graphics.

32 **Conflicts of interest**
33 All authors report no competing financial interests or potential conflicts of interest.

34 **Funding sources**
35 This work was supported by the National Institute on Drug Abuse award numbers DA041482 (A.R.T.),
36 DA047678 (A.R.T.) and a Brain and Behavior Research Foundation Young Investigator Award (S.M.).
37 The content is solely the responsibility of the authors and does not necessarily represent the official views
38 of the National Institutes of Health.

eNeuro Accepted Manuscript

39

40 **Abstract**

41 Midbrain dopaminergic (DAergic) neurons of the ventral tegmental area (VTA) are engaged by
42 rewarding stimuli and encode reward prediction error to update goal-directed learning. However, recent
43 data indicate VTA DAergic neurons are functionally heterogeneous with emerging roles in aversive
44 signaling, salience, and novelty, based in part on anatomical location and projection, highlighting a need
45 to functionally characterize the repertoire of VTA DAergic efferents in motivated behavior. Previous
46 work identifying a mesointerpeduncular circuit consisting of VTA DAergic neurons projecting to the
47 interpeduncular nucleus (IPN), a midbrain area implicated in aversion, anxiety-like behavior, and
48 familiarity, has recently come into question. To verify the existence of this circuit, we combined
49 presynaptic targeted and retrograde viral tracing in the dopamine transporter (DAT)-Cre mouse line.
50 Consistent with previous reports, synaptic tracing revealed axon terminals from the VTA innervate the
51 caudal IPN; whereas, retrograde tracing revealed DAergic VTA neurons, predominantly in the paranigral
52 region, project to the nucleus accumbens shell, as well as the IPN. To test if functional DAergic
53 neurotransmission exist in the IPN we expressed the genetically encoded DA sensor, dLight 1.2, in the
54 IPN of C57Bl/6J mice and measured IPN DA signals in vivo during social and anxiety-like behavior using
55 fiber photometry. We observed an increase in IPN DA signal during social investigation of a novel but
56 not familiar conspecific and during exploration of the anxiogenic open arm of the elevated plus maze.
57 Together, these data confirm VTA DAergic neuron projections to the IPN and implicate this circuit in
58 encoding perceived motivated exploration.

59 **Significance Statement**

60 Ventral tegmental area (VTA) dopamine (DA) neurons respond to reward but can also be engaged by
61 aversive stimuli highlighting the need to functionally characterize VTA projections to understand how
62 DA signaling underlies motivated behavior. Previous studies identified VTA DA neurons that project to

eNeuro Accepted Manuscript

63 the interpeduncular nucleus (IPN) where they modulate anxiety and novelty preference. In mice, the
64 existence of IPN-projecting VTA DA neurons was confirmed using viral tracing. Expressing a genetically
65 encoded DA sensor in the IPN and monitoring DA revealed that IPN DA is increased in response to novel
66 and anxiogenic stimuli. These data verify that a small population of DA neurons in the VTA project to the
67 IPN where they are engaged during motivated exploration.

68 **Introduction**

69 The modulatory neurotransmitter dopamine (DA) plays critical roles in reward, learning, motivation and
70 action selection (Arber and Costa, 2022; Berridge and Robinson, 1998; Floresco, 2015; Schultz et al.,
71 1997). Despite decades of intense research, the precise regulation, and the circuitry architecture of
72 DAergic neurotransmission still remains unclear (Berke, 2018). Growing evidence demonstrate that
73 midbrain DAergic systems are integrated by a spectrum of molecularly, anatomically and functionally
74 distinct neuron subtypes. In addition, single-cell gene expression profiling (Phillips et al., 2022; Poulin et
75 al., 2020; Tiklová et al., 2019), together with projection specificity functional mapping, support the
76 hypothesis that heterogeneous DA neuronal clusters can influence individual behavioral readouts
77 (Lammel et al., 2014; Morales and Margolis, 2017; Poulin et al., 2018).

78 Midbrain DA neurons in the ventral tegmental area (VTA) respond to reward (Mirenowicz and Schultz,
79 1996), reward-predictive cues (Flagel et al., 2010), associative learning (Saunders et al., 2018), as well as
80 salient stimuli, such as novel social investigations (Gunaydin et al., 2014; Solié et al., 2021). In addition,
81 some VTA DA neurons are engaged by aversive stimuli (Matsumoto and Hikosaka, 2009) or during
82 anxiety and fear-related behaviors (Zweifel et al., 2011). Most VTA DA neurons send abundant
83 projection-specific outputs to the ventral striatum nucleus accumbens region (NAc), where they regulate
84 reward-related and aversive processing (de Jong et al., 2019; Lammel et al., 2012), encode saliency (Kutlu
85 et al., 2021) or promote social behaviors (Gunaydin et al., 2014), but whether the same neurons send

eNeuro Accepted Manuscript

86 functional projections to additional areas and how they control emotional and motivational behaviors is
87 not fully understood.
88 Medial and ventral adjacent to the VTA resides the interpeduncular nucleus (IPN) of the midbrain. The
89 IPN receives excitatory inputs from the epithalamic medial habenula (mHb) and sends efferent projections
90 to midbrain and hindbrain structures including the raphe, tegmentum and pontine nucleus (Groenewegen
91 et al., 1986; Lima et al., 2017). IPN neurons are predominantly GABAergic, although IPN glutamatergic
92 and serotonergic neurons have also been reported (Quina et al., 2017; Sherafat et al., 2020). Anatomically,
93 the IPN has been subdivided into 3 unpaired and 4 paired subnuclei: the median, unpaired subnuclei
94 include the apical (IPA), rostral (IPR) and central (IPC) nuclei, whereas the paired subnuclei involve the
95 dorsolateral (IPDL), dorsomedial (IPDM), lateral (IPL) and intermediate (IPI) subnuclei (Hemmendinger
96 and Moore, 1984). The cytoarchitecture, molecular profiling and functional connectivity of distinct IPN
97 neuronal clusters is largely unknown.
98 Increasing attention has focused on the mHb-IPN axis over the last two decades, as it highly expresses
99 a unique combination of nicotinic acetylcholine receptor (nAChR) subunits, α5, α3 and β4, encoded
100 within the *CHRNA5-A3-B4* gene cluster (Improgo et al., 2010), extensively associated with nicotine
101 dependence in human genetic studies (Berrettini et al., 2008; Bierut et al., 2008). Numerous investigations
102 in rodents have corroborated the role of the mHb-IPN circuit as key regulator of nicotine intake (Fowler
103 et al., 2011; Frahm et al., 2011) and of nicotine withdrawal, including both physical and affective aspects
104 (Antolin-Fontes et al., 2015; Casserly et al., 2020; Görlich et al., 2013; Klenowski et al., 2021; Salas et
105 al., 2009; Zhao-Shea et al., 2015, 2013). Emerging evidence further implicates this axis in regulating fear-
106 related memories as well as baseline anxiety-like behaviors (Molas et al., 2017a; Seigneur et al., 2018;
107 Soria-Gómez et al., 2015; Yamaguchi et al., 2013; J. Zhang et al., 2016).
108 Recent data described a mesointerpeduncular pathway consisting of VTA DAergic neurons that
109 innervate the IPN (Zhao-Shea et al., 2015), a circuit that mediates anxiety-like behavior through unique

110 IPN microcircuitry (DeGroot et al., 2020) and that controls the motivational component of familiar social
111 investigations (Molas et al., 2017b). Such crosstalk between two adjacent midbrain structures with
112 apparent opposing roles in regulating behavior (Wills et al., 2022) could have important implications for
113 balancing motivational and affective behaviors. However, a recent study excluded the existence of an
114 anatomic connection from the VTA to the IPN (Nasirova et al., 2021). Thus, a comprehensive analysis
115 clarifying VTA DAergic neuron connections to the IPN and elucidating internal signals that trigger DA
116 release in this brain area, would provide valuable insight into VTA DA neuron architecture, as well as
117 intrinsic midbrain DA circuitry function.

eNeuro Accepted Manuscript

eNeuro Accepted Manuscript

118 **Materials and Methods**

119 **Animals**

120 All animal experiments were conducted in accordance with the guidelines for care and use of laboratory
121 animals provided by the National Research Council, and with approved animal protocols from the
122 Institutional Animal Care and Use Committee of the Institution. C57BL/6J (Stock #000664,
123 https://www.jax.org/strain/000664) and DAT-Cre (Stock #006660, https://www.jax.org/strain/006660)
124 mice were obtained from the Jackson Laboratory and bred in the institution animal facility. Cre lines were
125 crossed with C57BL/6J mice and only heterozygous animals were used for the experiments. Mice of both
126 sexes were used in all experiments. For social experiments, juvenile stimuli always consisted of C57Bl/6J
127 mice (4-7 weeks old). Mice were group housed with a maximum of five per cage and were kept on a
128 standard 12 h light/dark cycle (light on at 7 A.M.) with *ad libitum* access to food and water. Following
129 viral brain injections and recovery overnight, mice for behavior experiments were transferred to the
130 reverse light/dark cycle room (light on at 7 P.M.) for 3 weeks prior to the fiber brain implantations or
131 further experiments. Mice were single house at least one week before behavior testing which were
132 conducted during the dark cycle (8 A.M. to 5 P.M.).

133 **Viral preparations**

134 Biosensors, optogenetic and control plasmids packaged into viral particles were purchased from Addgene.
135 For tracing experiments we used pAAV.hSyn.mCherry (#114472-AAV2, 2.6 x 10^{13} GC/ml,
136 https://www.addgene.org/114472/), pAAV.hSyn.DIO.EGFP (#50457-AAVrg, 1.4 x 10^{13} GC/ml,
137 https://www.addgene.org/50457/), pAAV-hSyn-Flex-mGFP-2A-Synaptophysin-mRuby (#71760-AAV1,
138 7.0 x 10^{11} GC/ml, https://www.addgene.org/71760/) and pAAV-hSynapsin1-Flex-axon-GCaMP6s
139 (#112010-AAV5, 2.2 x 10^{13} GC/ml, https://www.addgene.org/112010/). For fiber photometry
140 experiments we used pAAV.hSyn.dLight1.2 (#111068-AAV5, 8.7 x 10^{12} GC/ml,

eNeuro Accepted Manuscript

141 https://www.addgene.org/111068/). Viral injections were performed on 6 weeks old mice and between 4
142 to 6 weeks were allowed for transgene expression.

143 **Stereotaxic surgeries**

144 Briefly, mice (6 weeks old) were deeply anaesthetized with a mixture of 100 mg/kg ketamine and 10
145 mg/kg xylazine (VEDCO) by intraperitoneal (IP) injection. Ophthalmic ointment was applied to maintain
146 eye lubrication. The skin of skull was shaved and disinfected with iodine. Mice were then placed on a
147 heating pad and in a stereotaxic frame (Stoelting Co.) and the skull was exposed by making a small
148 incision with a scalpel blade. Using bregma and lambda as landmarks, the skull was leveled along the
149 coronal and sagittal planes. A 0.4-mm drill was used for craniotomies at the target Bregma coordinates.
150 Microinjections were made by using a gas-tight 33G Hamilton 10 µl neurosyringe (1701RN, Hamilton)
151 and a microsyringe pump (Stoelting Co.). The following coordinates (in mm, Bregma anterioposterior
152 (AP), mediolateral (ML) and dorsoventral (DV)) were used for nucleus accumbens, AP 1.0, ML +/- 0.5,
153 DV -4.0; VTA, AP -3.51, ML +/- 0.2, DV -4.2; IPN, AP -3.51, ML -1, DV -4.81 and 12° angle. Viral
154 volumes for injections were 300 nl, delivered at a constant flow rate of 30 nl/min. After injection, the
155 needle was left unmoved for 10 min before being slowly retracted. The incision was then closed and held
156 together with Vetbond.

157 After 3 weeks recovery from virus injection, mice underwent surgery as described above for implantation
158 of optic fibers. Optic fiber (200 µm core diameter; 0.48 N.A., Doric Lenses) was placed targeting the IPN
159 (AP -3.8, ML -1, DV -4.61, 12.5°) and was held in place with adhesive luting cement (C&B metabond,
160 Parkell Inc.) followed by dental cement (Cerebond, PlasticsOne). Mice were allowed to recover for 5 to 7
161 days in the reverse light/dark cycle room before behavior tests. Injection sites and viral expression were
162 confirmed for all animals by experimenters blinded to behavioral outcome as previously described (Molas
163 et al., 2017b). Animals showing no viral or off-target site viral expression or incorrect optic fiber
164 placement (< 10%) were excluded from analysis.

eNeuro Accepted Manuscript

165 **Fiber photometry and data analysis**

166 Florescent signals from biosensors were recorded with a Doric Instruments Fiber Photometry System. An
167 LED driver was used to deliver excitation light from LEDs at 465 nm (~8.5 mW output) and at 405 nm
168 (~5 mW output), which was used as an isosbestic wavelength for the indicator (Doric Instruments). The
169 light was reflected into a 200 µm 0.48 N.A. optic fiber patch cord via the Dual Fluorescence Minicube
170 (Doric Instruments). Emissions were detected with a femtowatt photoreceiver (Model 2151, Newport) and
171 were amplified by transimpedance amplification to give an output voltage readout. Sampling (12 kHz)
172 and lock-in demodulation of the fluorescence signals were controlled by Doric Neuroscience Studio
173 software with a decimation factor of 50. A Doric behavior camera was connected to the Doric
174 Neuroscience Studio software using USB 3.0 Vision interface to synchronize the photometry recordings
175 with time-locked behavioral tracking systems. All mice were habituated to the patch cord plugged to the
176 optic fiber implant for 10 min in their home cages prior to the start of the experiment. For social novelty
177 tests, recordings began with the animal in the home cage for 1 min and then was placed by the
178 experimenter to the center of the behavioral apparatus. Behavioral events were tallied from the videos in
179 a blinded fashion and analysis was done using the time-locked photometry recording.

180 Fiber photometry data analysis was performed using custom-written Matlab scripts. A lowpass filter (3Hz)
181 was applied to the demodulated fluorescence signals before the 405 nm channel was scaled to the 465 nm
182 by applying a least mean squares linear regression. Scaled signals were used to calculate the $\Delta F/F_0$ where
183 $\Delta F/F_0$ = (465 nm signal – fitted 405 nm signal)/fitted 405 nm signal. Z-scores were calculated using as
184 baseline the average $\Delta F/F_0$ values from the -1.0 s prior to the onset of each behavioral event (considered
185 as time zero, t=0). For random sampling, two sets of 10 start timestamps were randomly generated, one
186 set within the first 5 to 149.99s and the other within 150-294.99 s of the 5 min recording trace. For the 20
187 random timestamps, $\Delta F/F_0$ were extracted from -1 to 3 s and the z-scores of each event estimated using
188 as baseline the -1.0 s prior to the timestamp.

eNeuro Accepted Manuscript

189 **Behavioral assays**

190 Animals were acclimated to the testing room for 30 min before any experimental assay, and all testing
191 was performed under dim red-light conditions.

192 Social behavior

193 Social behavior experiments were performed in wild-type C57BL/6J mice expressing the dLight1.2
194 biosensor in the IPN. Both in male and female mice were used, which interacted with a same-sex
195 C57BL/6J juvenile conspecific. Animals were tested in a plexiglass apparatus (42 x 64 x 30 cm) containing
196 two plastic grid cylinders (25 cm x 10 cm diameter) located at opposite corners of a rectangular maze.
197 Subject mice were first habituated to the apparatus and the empty cylinders for a 5-min period. Following
198 habituation, a juvenile unfamiliar C57BL/6J conspecific (4-7 weeks of age) was placed inside one of the
199 two cylinders (counterbalanced), reducing social investigations led by the subject animals. The subject
200 mouse was then positioned in the central zone and allowed to freely explore the social and non-social
201 cylinders for 5 min. This testing phase was repeated 24h, on day 2, using the same juvenile conspecific
202 located in the same compartment which became familiar. The apparatus and cylinders were cleaned with
203 Micro-90 solution (International Products Corporation) to eliminate olfactory traces after each session.
204 All sessions were video recorded and synchronized to activity dynamics. Exploration of the social and
205 non-social cylinders in videos of the trials were labeled frame by frame by experimenters blind to group
206 conditions. Onset of each behavioral exploratory event (considered as t=0) was defined whenever the
207 subject mouse directed its nose towards the cylinders at a distance < 2 cm and initiated a sniffing
208 investigation. Sitting or resting next to the cylinder or objects was not considered exploration.

209 Elevated plus maze

210 The elevated plus maze (EPM) apparatus consisted of a central junction (5 × 5 cm), four arms elevated 45
211 cm above the floor with each arm positioned at 90° relative to the adjacent arms. Two closed-arms were
212 enclosed by high walls (30 × 5 × 15 cm) and the open-arms were exposed (30 × 5 × 0.25 cm). A 60W red

eNeuro Accepted Manuscript

213 fluorescent light was positioned 100 cm above the maze and was used as illumination source. Both male
214 and female C57BL/6J mice expressing the DA biosensor dLight1.2 in the IPN were used. The optic fiber
215 implant was connected to the recording patch cord, and then mice were placed on the junction part of the
216 maze facing one of the open arms. All mice were given 5 min of free exploration while their behavior was
217 video-recorded and synchronized to the dLight1.2 signals via the Doric instruments fiber photometry
218 system, as described above.

219 **Immunostaining and microscopy**

220 Mice were euthanized by i.p injection of sodium pentobarbital (200 mg/kg) and transcardially perfused
221 with ice cold 0.1 M phosphate buffer saline (PBS, pH 7.4) followed by 10 ml of cold 4% (W/V)
222 paraformaldehyde (PFA) in 0.1 M PBS. Brains were post-fixed in 4% PFA for 2 h and then submerged in
223 30% sucrose. Brains were sliced to coronal sections (25 μm) by using a freezing microtome (HM430,
224 Thermo Fisher Scientific). For virus expression and fiber implants verification, after washes in 0.1 M
225 PBS, sections were mounted, air-dried and coverslipped with Vectashield mounting medium (Vector
226 Laboratories). Slices were imaged using a fluorescence microscope (Zeiss, Carl Zeiss MicroImmagine,
227 Inc.) connected to computer-associated image analyzer software (Axiovision Rel., 4.6.1). For
228 immunohistochemical staining, brain sections were permeabilized with 0.2% Triton X-100 in 0.1 M PBS
229 for 5 min, blocked with 2% BSA in 0.1 M PBS for 30 min and then incubated overnight with the
230 corresponding primary antibodies in 2% BSA at 4°C. Primary antibodies used: mouse anti-TH 1:500
231 (Millipore, MAB318, https://www.emdmillipore.com/US/en/product/Anti-Tyrosine-Hydroxylase-
232 Antibody-clone-LNC1,MM_NF-MAB318), guinea pig anti-synaptophysin 1:300 (alomone labs, AGP-
233 144, https://www.alomone.com/p/guinea-pig-anti-synaptophysin-antibody/ANR-013-GP). Slices were
234 subsequently washed in 0.1 M PBS, blocked with 2% donkey (or goat) serum (Sigma) for 30 min and then
235 incubated in secondary antibodies for 1 h (1:800; Life Technologies; donkey anti-mouse 647 (A31571),
236 goat anti-guinea pig 594 (A11076)). After washes in 0.1 M PBS, sections were mounted, air-dried and

eNeuro Accepted Manuscript

237 coverslipped with Vectashield medium with DAPI (Vector Laboratories). Images were obtained by a Zeiss
238 LSM 700 confocal microscope at 10x or at 10x with a 1.5 zoom. Images were analyzed using ImageJ Fiji
239 to create a zoomed-in inset (the red line square on the images, with a 1.5 or 2 zoom factor). The ImageJ
240 JAcoP method was used for co-localization analysis between VTA^{DA}→IPN fibers expressing
241 AxonGCaMP and synaptophysin staining. Briefly, each image threshold was set automatically for analysis
242 before Manders' coefficient was applied to obtain the fraction of synaptophysin (red) overlapping with
243 VTA^{DA}→IPN terminals (green) and vice versa. For quantification of fluorescently labeled axons from
244 VTA^{DA} neurons innervating the IPN, the Digital Enhancement of Fibers with Noise Elimination
245 (DEFiNE) method was applied (Powell et al., 2019), available for download
246 here: https://figshare.com/s/1be5a1e77c4d4431769a. Axons were quantified in confocal images that
247 were not processed through the clean images function, but each input image was a single–channel
248 maximum intensity projection. Quantification was performed in ROIs (0.3 mm x 0.4 mm) randomly
249 allocated within the anterior (Bregma -3.4mm) and posterior (Bregma -3.8mm) IPN.

250 **Statistical analysis**

251 Statistical analyses for fiber photometry were done using parametric tests on z-scored data after testing
252 for normality. One-way or two-way repeated measures (RM) ANOVA with Dunnett's multiple
253 comparisons tests or Bonferroni post-hoc tests were conducted for the analyses involving the comparison
254 of group means as indicated. Z-scores are presented as mean ± SEM of all events for transitions between
255 open (included junction) and closed arms and for social approach behaviors. Comparisons of z-scores
256 were made using the calculated average for each animal. All analyses were performed using Prism 9
257 (Graphpad, San Diego, CA). Statistical significance was accepted at $P < 0.05$.

258

259 **Code Accessibility**

eNeuro Accepted Manuscript

260 The code used for fiber photometry data analysis is freely available on GitHub
261 (https://github.com/TapperLab/TapperLab)
262

eNeuro Accepted Manuscript

263 **Results**

264 We used a genetic strategy to target putative DA neuron subtypes and rigorously investigate DAergic
265 projections from the VTA to the neighboring IPN. To this aim, we specifically selected a knock-in genetic
266 mouse line that expresses Cre recombinase under the transcriptional control of the endogenous dopamine
267 transporter (DAT) promoter. In this mouse line, Cre recombinase expression is driven from the 3'
268 untranslated region (3' UTR) of the endogenous DAT gene by means of an internal ribosome entry
269 sequence (IRES), to reduce interference with DAT function (Bäckman et al., 2006). Some neurons in the
270 IPN express tyrosine hydroxylase (*Th*) mRNA, which can lead to recombination in *Th*-IRES-Cre mice,
271 although these neurons have low/undetectable TH protein in the adult brain (Poulin et al., 2018). These
272 Th^+ IPN neurons are not related to midbrain DA neurons, as they are not derived from the midbrain floor
273 plane, and they lack the expression of typical DAergic neuronal markers such as DAT, NURR1, FOXA2
274 or PITX3 (Poulin et al., 2018), thereby using DAT-Cre mice restricts and minimizes expression to
275 midbrain DA neurons. Previous work expressed a Cre-dependent virus in the VTA of DAT-Cre animals
276 and detected neuronal projections innervating mainly the caudal part of the IPN (cIPN) (DeGroot et al.,
277 2020; Molas et al., 2017b). To verify that VTA^{DA}→IPN projections are indeed axonal terminals and not
278 simply DA dendritic elements extending into the IPN, we injected AAVs containing the
279 hSyn.Flex.mGFP.2A.synaptophysin.mRuby construct into the VTA of DAT-Cre mice (Fig. 1A).
280 Following Cre recombination, synaptophysin fused to the mRuby red fluorophore is selectively
281 transported into the axonal compartments of the transfected neurons (Fig. 1A)(S. Zhang et al., 2016). TH
282 immunostaining demonstrated efficient recombination restricted to DA neurons in the midbrain (Fig. 1B).
283 Furthermore, via circuit-mapping, abundant axon terminals were detected in the nucleus accumbens
284 (NAc) region, the principal output target of VTA^{DA} neurons (Fig. 1C). These VTA^{DA}→NAc axon
285 terminals intensely expressed synaptophysin-mRuby fused protein (Fig. 1C), altogether validating the
286 viral-mediated genetic strategy. To delineate the VTA^{DA}→IPN circuit, we used a group of 6 mice, with

eNeuro Accepted Manuscript

287 comparable results. All injected animals reliably exhibited VTA^{DA} synaptophysin-mRuby axon terminals
288 innervating the IPR region of the cIPN (Fig. 1 D). Additional VTA^{DA} axonal varicosities were also
289 detected targeting the cIPN IPDM/IPDL subregion (Fig. 1D), consistent with previous data (DeGroot et
290 al., 2020; Molas et al., 2017b).

291 To reassure that VTA DA neurons send neuronal projections innervating the neighboring IPN and that
292 these are active presynaptic axons, DAT-Cre mice received an injection of Cre-dependent AxonGCaMP
293 in the VTA expressed via AAV5-mediated gene delivery (Fig. 2A). This genetically encoded calcium
294 indicator is uniformly enriched in axons, allowing for structure-specific labeling of presynaptic terminals
295 (Broussard et al., 2018). Similarly, as described above, presynaptic terminals from VTA^{DA} neuronal inputs
296 were observed in the IPR and IPDM regions of the cIPN (Fig. 2B-D). Moreover, immunostaining against
297 synaptophysin protein revealed robust co-localization between the GFP+ (AxonGCaMP) and
298 synaptophysin (Fig. 2B-D), confirming active presynaptic structures.

299 Distinct VTA^{DA} projection populations regulate reward associations and motivation via specific NAc
300 inputs (Heymann et al., 2020). To elucidate the projection-specificity of VTA^{DA} that innervate the cIPN,
301 DAT-Cre mice received a co-injection of AAV2-hsyn-mCherry (localization marker) together with
302 AAVrg-hsyn-DIO-eGFP into the NAc region (Fig. 3A). Imaging of the target injection site confirmed
303 viral-mediated gene delivery restricted mainly in the shell area of the NAc (Fig. 3B). In addition, to verify
304 the retro-labeled neurons detected in the VTA were positive for DAergic markers, brain slices of the
305 injected animals were immuno-stained against TH protein. All the experimental animals (n = 6 mice)
306 exhibited abundant terminal projections from retro-labeled VTA→NAc projecting neurons that innervated
307 the IPR region of the cIPN (Fig. 3C). The cell bodies from VTA→IPN projecting neurons mostly localized
308 in the paranigral (PN) area of the VTA (Fig. 3C) and were indeed DAergic, as shown by co-localization
309 with TH staining (Fig. 3C). For visualization enhancement and quantification of the fluorescently labeled
310 axons we used the DEFiNE method. Axonal fibers innervating the IPN from retro-labeled VTA^{DA}→NAc

eNeuro Accepted Manuscript

311 projecting neurons were highly enriched in posterior regions of the IPN (cIPN) as compared to anterior
312 IPN Bregma (Fig. 4A-B). Similarly, quantification of axonal fibers originating from direct infusion of the
313 synaptophysin-mRuby construct in VTA^{DA} neurons revealed increased axon terminals at more posterior
314 IPN Bregma compared to anterior (Fig.4C-D). Noticeably, in anterior IPN Bregma, the number of axonal
315 fibers was higher when VTA^{DA} neurons were directly transfected with the synaptophysin-mRuby
316 construct as opposed to retro-labeled VTA^{DA}→NAc projecting neurons (Fig. 4E). In contrast, these two
317 viral-mediated VTA^{DA} neuron labeling strategies resulted in similar number of axonal fibers at posterior
318 IPN Bregma (Fig. 4F).

319 Previous work suggested that the VTA^{DA}→IPN circuit is engaged during anxiety-like behaviors
320 (DeGroot et al., 2020) and when mice encounter unfamiliar conspecifics (Molas et al., 2017b). Although
321 DA signals have been detected in acute mouse IPN slices (DeGroot et al., 2020), the real-time dynamics
322 of *in vivo* IPN DAergic neurotransmission have never been reported. To this aim, here we recorded IPN
323 DA dynamics in freely behaving mice using the genetically encoded DA sensor dLight1.2 (Patriarchi et
324 al., 2018). Fluctuations in IPN DA signals were recorded during the 3-chamber sociability task, when
325 mice encountered a new juvenile conspecific (Fig. 5A and Methods). On the following day, subject mice
326 were presented to the same juvenile conspecific in the same location, which became familiar (Fig. 5A and
327 Methods). To this aim, we virally expressed dLight1.2 in the IPN of C57BL/6J mice, enabling ultrafast
328 optical DA recordings, and three weeks post-viral transduction we implanted an optic fiber targeting the
329 injection site (Fig. 5B). IPN DA dynamics were time-locked to when animals approached and initiated a
330 sniffing investigation of conspecific stimuli (Fig. 5C). Demodulated fluorescence signals were obtained
331 from the 465 and 405 nm channels in a 5 min trial (Fig. 5D). The 405 nm channel was scaled to the 465
332 nm by applying a least mean squares linear regression (Fig. 5E). Scaled signals were used to calculate the
333 $\Delta F/F_0$ where $\Delta F/F_0$ = (465 nm signal – fitted 405 nm signal)/fitted 405 nm signal (Fig. 5F). On day 1 of
334 the sociability test, sniffing investigation of a novel conspecific significantly increased the release of DA

eNeuro Accepted Manuscript

335 in the IPN (Fig. 5G-I). However, IPN DA signals rapidly habituated on the next session, as the conspecific
336 became familiar (Fig. 5J-L). Random sampling IPN DA signals without being time-locked to social
337 sniffing investigations did not result in apparent changes in activity neither when mice interacted with a
338 novel conspecific (Fig. 5M-O) nor when this became familiar (Fig. 5P-R).

339 To further investigate IPN DA signals trigger by additional behaviors, we recorded IPN DA dynamics
340 in mice tested in the elevated plus maze (EPM)(Fig. 6A), a well-established paradigm to measure anxiety-
341 like behaviors in rodents (Walf and Frye, 2007). As mice investigated the open arms of the EPM, the
342 release of DA in the IPN significantly increased (Fig. 6B-E). Conversely, the transition from the open to
343 the closed EPM compartments led to reductions in IPN DA signals (Fig. 6B, F-H). Time-locked IPN DA
344 signals when mice entered the open arms were higher as compared to when entering the closed arms of
345 the EPM or to non-time locked random sampling signals (Fig. 6I-K). All the recorded animals were
346 verified for correct viral expression and fiber placement within the cIPN (Fig. 7).

eNeuro Accepted Manuscript

347 **Discussion**

348 DA dysfunction has been implicated in numerous brain diseases, including addiction,
349 depression, schizophrenia, Parkinson's disease, and anxiety disorders (Horga and Abi-Dargham, 2019;
350 Nestler and Lüscher, 2019; Ruitenberg et al., 2021; Taylor et al., 2021; Zalachoras et al., 2022). A
351 comprehensive understanding of the circuit architecture and the functional mapping of DA neurons is
352 imperative to gain insights into inherent regulation of DA neurotransmission in health and disease. The
353 present study confirms the existence of a mesointerpeduncular pathway that connects the VTA with the
354 IPN, thereby modulating behavioral states with implications in overall midbrain DA circuitry function.

355 Viral mediated circuit tracing replicated previous findings (DeGroot et al., 2020; Molas et al., 2017b;
356 Zhao-Shea et al., 2015), validating anatomical connections between VTA DAergic neurons and the IPN.
357 The current work used the DAT-Cre knock-in mouse line, in which Cre mimics the expression pattern of
358 the plasma membrane dopamine transporter (Bäckman et al., 2006; Lammel et al., 2015) and therefore,
359 demonstrates higher specificity targeting putative midbrain DA neurons (Poulin et al., 2018). VTA DA
360 axons preferentially innervated the IPR region of the cIPN, as previously reported. These axon terminals
361 were detected in most injected animals across multiple experimental cohorts and appeared to be more
362 obvious in those mice where viral expression extended to the PN region of the VTA. In addition,
363 synaptically targeted markers localized in terminal projections from the VTA^{DA}→IPN circuit, whereby
364 protein immunostaining revealed active presynaptic terminals rather than passing fibers. Interestingly, the
365 cIPN is highly enriched in neurons expressing the D1 receptor (Molas et al., 2017b), but also in
366 serotonergic cell bodies (Groenewegen et al., 1986). Serotonergic IPN neurons innervate the ventral
367 hippocampus (vHipp) to mediate active stress coping and natural reward (Sherafat et al., 2020).
368 Considering that cIPN neurons can amplify VTA^{DA} signals through a microcircuit that spans to additional
369 IPN subregions (DeGroot et al., 2020), if some of these cIPN neurons comprise the serotonergic

eNeuro Accepted Manuscript

370 IPN→vHipp pathway, then the VTA^{DA} signal would amplify to more distant regions to control
371 motivational and affective behaviors.

372 Anatomical and functional connectivity of midbrain DA neurons has been broadly investigated across
373 animal species (Morales and Margolis, 2017; Swanson, 1982). Numerous studies identified the source of
374 synaptic input to DA neurons (Beier et al., 2015; Lammel et al., 2012; Watabe-Uchida et al., 2012), as
375 well as output targets (Heymann et al., 2020; Lammel et al., 2011, 2008; Poulin et al., 2018). While
376 consistent data indicate the NAc is the major target of VTA DA neurons, additional structures such as the
377 amygdala, cortex, hippocampus, ventral pallidum, septum, periaqueductal grey, bed nucleus of stria
378 terminalis, olfactory tubercle and locus coeruleus, among others, also receive DAergic inputs from the
379 VTA. Noticeably, most of the circuit tracing studies traditionally focus on those regions with highest
380 abundance of DA terminal projections, neglecting target specific sites that receive sparse DAergic inputs.
381 For instance, VTA neurons send local, topographically organized axonal connections that innervate the
382 VTA itself (Adell and Artigas, 2004; Aransay et al., 2015; Ferreira et al., 2008), which overall have
383 received less attention. Of note, Aransay et al, also reported VTA innervation to the IPN, although less
384 frequent (Aransay et al., 2015), nevertheless supporting a direct anatomical link between the VTA and
385 IPN.

386 The anatomical location of DA neuron synaptic output can be a critical factor determining its intrinsic
387 properties and behavioral outcomes (de Jong et al., 2019; Lammel et al., 2011). Our data show that a
388 subpopulation of NAc shell-projecting VTA DA neurons in the PN region may preferentially project into
389 the IPN to innervate cIPN, as reported previously (DeGroot et al., 2020). Emerging evidence suggest that
390 subpopulations of VTA DAergic neurons can innervate more than one brain structure (Aransay et al.,
391 2015). Specifically, medial shell NAc-projecting DA neurons send significant collaterals outside the
392 striatum, including the septum and ventral pallidum, indicating that this DA subpopulation is capable of
393 simultaneously influencing neural activity in multiple brain regions (Beier et al., 2015). Since the same

eNeuro Accepted Manuscript

394 DA neurons presumably innervate the IPN, the data together position the IPN as an integral member within
395 specific VTA DAergic sub-circuitries.

396 Our photometry results demonstrate that innate DA signals in the IPN are triggered with motivated
397 exploration, when mice investigate novel conspecific individuals and when they explore the anxiogenic
398 arms of the EPM. These results affirm that social interactions bear rewarding aspects and recruit neural
399 circuits of motivation (Chevallier et al., 2012), including DAergic systems (Bariselli et al., 2018;
400 Gunaydin et al., 2014; Hung et al., 2017; Solié et al., 2021). Given the NAc shell represents a storage site
401 for social memories (Okuyama et al., 2016), one possibility could be that innate IPN signals contribute to
402 social novelty and familiarity responses, supporting previous findings (Molas et al., 2017b). On the other
403 hand, NAc shell-projecting VTA DA neurons are recruited by aversive stimuli and cues that predict them
404 (de Jong et al., 2019). Increased IPN DA signals with the exploration of anxiogenic environments would
405 result from activation of a neural network that strengthens responses to aversive stimuli to modulate
406 anxiety-like behavior.

407 A recent study excluded the existence of an anatomic connection from the VTA to the IPN (Nasirova et
408 al., 2021). One possible explanation for the discrepancy in the results may be that most of the viral-
409 mediated circuit tracing in the study of Nasirova et al., was done in a Cre mouse line that only targets IPN
410 neurons expressing the α5 nAChR subunit. Although neurons in the IPN are highly enriched in α5*-
411 nAChRs (Ables et al., 2017), some subpopulations do not express the α5-encoding gene. Thus, limiting
412 IPN circuit tracing to an α5-expressing neuronal subtype does not accurately reflect total IPN connectivity.
413 In addition, for the viral-mediated retrograde tracing analysis, the authors selected IPN brain slices with a
414 maximum IPN caudal bregma coordinate of -3.6 mm according to the Paxinos atlas (Paxinos and Franklin,
415 2001) (Nasirova et al., 2021). As mentioned above, VTA DA neurons that project to the IPN localize more
416 caudal, at coordinates -3.63 to -4.03 mm from bregma, which were likely missed in the analysis.
417 Noticeably, previous work using rabies tracing from overall IPN neurons did detect sparse cell bodies

eNeuro Accepted Manuscript

418 localized in caudal VTA (Lima et al., 2017). Nasirova et al., utilized the Allen Connectivity Atlas to
419 reinforce their negative data. However, the few Allen examples performed in the Slc6a3-Cre (DAT-Cre)
420 line lack viral expression transfecting caudal VTA PN neurons, thereby precluding the detection of any
421 putative VTA^{DA} innervation to the IPN. Additionally, Nasirova et al. included examples of VTA Cre-
422 mediated anterograde tracing in DAT-Cre mice, but, for this experiment, the authors used a non-validated
423 Cre-dependent synaptically-targeted GFP marker, which presented strong labelling of cell bodies in the
424 medial mamillary nucleus and also the IPN itself (Nasirova et al., 2021), two brain regions lacking DA
425 neurons, thus raising questions regarding the specificity of the virus and therefore the validity of the
426 results. Surprisingly, the paper of Nasirova et al (2021) failed to cite, consider, or discuss DeGroot et al
427 (2020), which used a multidisciplinary approach and specifically demonstrated: 1) DA detection in IPN
428 slices using a genetically encoded DA sensor, 2) optogenetic activation of VTA DA IPN inputs elicits a
429 post-synaptic response that is blocked by a D1 receptor antagonist, 3) retrograde Cre-dependent AAV-
430 eGFP injection into the medial nucleus accumbens shell labels VTA neurons that clearly project into the
431 IPN of DAT-Cre mice (a result that was repeated here with the addition of TH staining to label DAergic
432 neurons), and 4) optogenetic activation or silencing the DAergic IPN input decreases and increases
433 anxiety-like behavior, respectively.

434 In summary, the present study was able to confirm the existence of a mesointerpeduncular pathway that
435 connects the VTA with the IPN, replicating previous findings (Aransay et al., 2015; DeGroot et al., 2020;
436 Molas et al., 2017b; Zhao-Shea et al., 2015). These results may significantly influence the prevailing
437 models of intrinsic midbrain DA circuitry as well as of IPN function. Considering that VTA DAergic
438 neurons also send projections to the mHb (Beier et al., 2015; Phillipson and Pycock, 1982), the data
439 together suggests a complex direct dopaminergic modulation of the habenulointerpeduncular tract that
440 may have strong impact on reward-related, aversive/affective motivated behaviors. Finally, beyond the
441 VTA-IPN axis, and bearing in mind that activation of small subsets of neuronal ensembles can lead to

eNeuro Accepted Manuscript

442 selective widespread activation of neural networks with concomitant behavioral outcome (Dalgleish et al., 443 2020; Marshel et al., 2019), the present work emphasizes the need of investigating sparse, functionally 444 relevant neglected circuits that may serve as signal amplification to computationally process motivational 445 information.

446 **Figure Legends**

447 **Fig 1. VTA DA neurons send axonal projections to the IPN**

448 **A**, Schematics depicting Cre-dependent recombination of the construct pAAV-hsyn-Flex-mGFP-2A-449 synaptophysin-mRuby in DAT-Cre mice and the viral injection strategy used. Dendritic arbors from a 450 Cre^{+} transfected neuron display exclusive mGFP green fluorescence, whereas mRuby red fluorescence 451 predominantly localizes in axon terminals. **B**, *Top*, representative image of viral injection in the VTA of 452 DAT-Cre mice, showing mGFP (green) and mRuby (red) expression in DA neurons immunolabeled with 453 TH staining (magenta). Nuclei are counterstained with DAPI (blue). *Bottom*, magnified view of the inset 454 region from the top image. White arrows show mGFP in dendritic arborizations and mRuby in axonal 455 projections from VTA^{DA} transfected neurons (Scale bars 100 µm). **C**, Representative image showing 456 mGFP and mRuby expression in efferents innervating the NAc from VTA^{DA} transfected neurons. (Scale 457 bars 100 µm). **D**, Illustrative drawing of the different interpeduncular (IP) subnuclei: apical (IPA), central 458 (IPC), dorsolateral (IPDL), dorsomedial (IPDM), intermediate (IPI), lateral (IPL) and rostral (IPR). IF, 459 interfascicular nucleus; ml, medial lemniscus; PN, paranigral nucleus; VTA, ventral tegmental area. All 460 cases # 1 to 6 (3 males, 3 females) show virally transfected neurons in the VTA co-labeled with TH 461 staining (scale bars 100 µm). Inset magnified views (red squares, 2x zoom in) demonstrate VTA^{DA} axon 462 terminals (mRuby+) innervating the IPR and also the IPDM/IPDL regions.

eNeuro Accepted Manuscript

463 **Fig 2. DAergic projections from the VTA to the IPN are presynaptic terminals.**

464 **A**, Schematic of viral-injection strategy in the VTA of DAT-Cre mice. **B**, Example of image showing
465 eGFP (AxonGCaMP) co-labeled with synaptophysin staining (red) in IPN. White arrows indicate
466 presynaptic puncta co-localization. *Inset*, magnified view of co-localization between eGFP and the
467 synaptophysin marker (scale bar 100 μm). **C,** Quantification of the co-localization coefficient between
468 eGFP and synaptophysin staining from single plane confocal images containing the cIPN (n = 6 mice, 4
469 males, 2 females). **D**, *Top*, AxonGCaMP expression in the VTA of DAT-Cre mice (eGFP, green),
470 synaptophysin immunostaining (red) and co-localization of the two channels (merge) in brain slices
471 containing the cIPN (scale bar 100 μm); *Bottom*, enlarged view of the IPR region from the top images
472 (gray square). White arrows denote VTA^{DA} eGFP+ presynaptic projections in the IPR co-localized with
473 synaptophysin puncta (scale bar 100 μm).

474 **Fig 3. VTA^{DA} neurons from the PN send projections to the IPN.**

475 **A**, Schematic of viral strategy used. DAT-Cre mice were injected with a viral mixture of AAV-hSyn-DIO-
476 eGFP (retrograde) and AAV2-hSyn-mCherry (location marker) (1:1) into the NAc. **B**, Representative
477 image showing the virus injection site targeting the NAc shell area (AcbSh) (scale bar 100 μm). **C**,
478 Example of injected animals, cases # 1 to 6 (4 males, 2 females), all showing retro-labelled eGFP+ neurons
479 in the VTA co-labeled with TH staining. For each case: *top*, TH immunostaining (magenta), retro-labelled
480 eGFP+ neurons from the NAc (green) and overlay of the two channels (merge) in brain slices containing
481 the cIPN (scale bar 100 μm). *Insets* in the *right* represent a magnified view enclosing the PN and IPR in
482 the merged channel (red square, 2x zoom in); *bottom*, enlarged view of the PN and IPR region from the
483 top images with a *right inset* image of the merge channel demonstrating AcbSh-projecting neurons in the
484 PN region are DAergic (TH+) and also send efferents to the IPR in the cIPN (red square, 2x zoom in)
485 (scale bar 100 μm).

eNeuro Accepted Manuscript

486 **Fig 4. DEFiNE quantification of fluorescently labeled axons from VTA^{DA} neurons to the IPN.**

487 **A,** Viral injection schematics (*left panel*) and representative images of axonal fibers innervating the IPN
488 from retro-labelled eGFP+ AcbSh-projecting VTA^{DA} neurons after DEFiNE processing at anterior (-3.40
489 mm) and more posterior (-3.80 mm) IPN Bregma (*right panel*). **B,** DEFiNE quantification of the retro-
490 labelled AcbSh-VTA^{DA} axonal fibers innervating the anterior and posterior IPN represented as total pixel
491 count (n = 6 mice, Unpaired two-tailed t-test ($t_{(10)}$ = 4.546, p = 0.0011)). **C,** Schematic of pAAV-hsyn-
492 Flex-mGFP-2A-synaptophysin-mRuby viral strategy used in DAT-Cre mice for labelling VTA^{DA} neurons
493 (*left panel*) with representative images of their axonal fibers innervating the IPN after DEFiNE processing
494 at anterior (-3.40 mm) and more posterior (-3.80 mm) Bregma (*right panel*). **D,** DEFiNE quantification of
495 the VTA^{DA} axonal fibers innervating the anterior and posterior IPN represented as total pixel count (n =
496 6 mice, Unpaired two-tailed t-test ($t_{(10)}$ = 3.438, p = 0.0064)). **E,** Comparison of axonal fibers in the
497 anterior IPN (Bregma -3.40 mm) quantified with the DEFiNE method when VTA DA neurons are directly
498 transfected with the pAAV-hsyn-Flex-mGFP-2A-synaptophysin-mRuby construct vs retro-labelled
499 eGFP+ AcbSh-projecting VTA^{DA} neurons (Unpaired two-tailed t-test ($t_{(10)}$ = 3.114, p = 0.011)). **F,** Same
500 comparison as (E) at IPN Bregma -3.80 mm (Unpaired two-tailed t-test ($t_{(10)}$ = 0.184, p = 0.8577)).

501 **Fig 5. Novel social encounters trigger IPN DA signals**

502 **A**, Schematic of the experimental approach used to measure IPN DA activity during interactions with
503 novel and familiar social stimuli. Subject mice were exposed to the same juvenile C57BL/6 conspecific
504 on day 1 (novel) and 2 (familiar) while IPN DA signals were recorded using the dLight biosensor. **B**,
505 Schematic of AAV-dLight viral injection strategy in the IPN of C57BL/6 mice (left panel) and
506 representative pictograph of DA sensor dLight1.2 (green) expression with optic probe location targeting
507 the cIPN (right panel) (scale bar 100 µm). **C**, Illustration of a social sniffing investigation. **D**, Example of
508 raw signals (Volts) corresponding to the 465 and 405 nm channels recording during a 5 min interaction
509 with a new social stimulus. **E,** The 405 nm channel is scaled to the 465 nm by applying a least mean

510 squares linear regression. **F,** Scaled signals are used to calculate the $\Delta F/F_0$ where $\Delta F/F_0$ = (465 nm signal
511 – fitted 405 nm signal)/fitted 405 nm signal. **G,** $\Delta F/F_0$ values time-locked to IPN DA signals relative to
512 the initiation of a social sniffing investigation (red line) on Day 1, when mice interact with a novel
513 conspecific. **H,** Heatmap representations (*top*) and z-score values (*bottom*) of the time-locked IPN DA
514 signals relative to social novelty explorations. **I**, average z-score per second compared to the baseline
515 signal from 1s prior to the onset of each social sniffing event (pre-onset, gray). Statistical comparisons
516 were made using an average z-score per animal (n = 10mice, 6 males, 4 females). Significant increases in
517 IPN DA activity were observed 2~3 s post-onset of novel social sniffing investigations. One-way repeated
518 measures (RM) ANOVA ($F_{(3,39)}$=21.80, P<0.0001). Dunnett's multiple comparisons test ** p<0.01, ***
519 p<0.001. **J**, $\Delta F/F_0$ values time-locked to IPN DA signals relative to the time initiating a social sniffing
520 investigation (red line) on Day 2, when mice interact with a familiar conspecific. **K**, Heatmap
521 representations (*top*), *z*-score values (*bottom*) of time-locked IPN DA signals relative to familiar social
522 explorations. **L**, Average z-score per second compared to the 1s baseline signal demonstrate no significant
523 change during familiar social sniffing investigations. One-way RM ANOVA ($F_{(3,39)}$=0.7103, P=0.517).
524 **M**, Example of IPN DA $\Delta F/F_0$ values time-locked to novel social investigations as compared to $\Delta F/F_0$
525 values obtained with random sampling across the 5 min recording session. **N,** Z-score values of (M). O,
526 Mean z-score values of the baseline and the 3 s novel social investigation event for the true signal as
527 compared to random sampling signal. Two-way RM ANOVA, significant time x z-score interaction
528 $F_{(1,29)}$=19.13, p=0.0001, Bonferroni post-hoc, ****p<0.0001. **P,** Example of IPN DA $\Delta F/F_0$ values time-
529 locked to familiar social investigations as compared to $\Delta F/F_0$ values obtained with random sampling
530 across the 5 min recording session. Q, Z-score values of (P). **R,** Mean z-score values of the baseline and
531 the 3 s familiar social investigation event for the true signal as compared to random sampling signal. All
532 data represent mean ± SEM.

eNeuro Accepted Manuscript

eNeuro Accepted Manuscript

533 **Fig 6. IPN DA signals are engaged with exploration of anxiogenic environments**

534 **A**, Schematic depicting fiber photometry recordings of IPN DA signals using the dLight1.2 biosensor in
535 the EPM test. **B**, Representative trace of IPN dLight1.2. fluorescence signals (dF/F0) when mice explored
536 the open arms (green) versus the closed arms (red) of the EPM. **C**, $\Delta F/F_0$ values time-locked to IPN DA
537 signals relative to the transition from the closed to the open arms of the EPM. **D**, Heatmap representations
538 (*top*) and *z*-score values (*bottom*) of time-locked IPN DA signals relative to the transition from the closed
539 to open arms of the EPM (gray line). **E**, Average z-score per second compared to the baseline signal from
540 1s prior to the exploration of the open arms. Statistical comparisons were made using an average z-score
541 per animal (n = 17 mice, 9 males, 8 females) that was calculated from all events. Significant increase in
542 IPN DA activity was observed 1~3s post-onset of open arm investigations. One-way RM ANOVA
543 ($F_{(3,67)}$=18.15, $P<0.0001$). Dunnett's multiple comparisons test ** $p<0.01$, *** $p<0.001$. **F**, $\Delta F/F_0$ values
544 time-locked to IPN DA signals relative to the transition from the open to the closed arms of the EPM. **G**,
545 Heatmap representations (*top*) and *z*-score values (*bottom*) of time-locked IPN DA signals relative to the
546 transition from the open to the closed arms of the EPM (gray line). **H**, Average z-score per second
547 compared to the baseline signal from 1s prior to the exploration of the closed arms. Significant decrease
548 in IPN DA activity was observed 1~3s post-onset of closed arm investigations. One-way RM ANOVA
549 ($F_{(3,67)}$=7.617, P=0.0042) Dunnett's multiple comparisons test * $p<0.05$, *** $p<0.001$. **I**, Example of IPN
550 DA $\Delta F/F_0$ values time-locked to the transition to the open or closed arms of the EPM as compared to
551 $\Delta F/F_0$ values obtained with random sampling across the 5 min recording session. J, Z-score values of (I).
552 **K,** Mean z-score values of the baseline and the 3 s open and closed EPM arm exploratory event for the
553 true signal as compared to random sampling signal. Two-way RM ANOVA, significant time x z-score
554 interaction $F_{(2,36)}$=4.14, p=0.024, p=0.0001, Bonferroni post-hoc, **p<0.001, ***p<0.001. All data
555 represent mean ± SEM.

556 **Fig 7. Distribution of fiber placement within the cIPN**

557 Schematics and representative images of dLight1.2 biosensor expression in the IPN of C57BL/6 mice with

558 examples of fiber placements distributed along the cIPN (Bregma -3.51 to -4.04 mm). Scale bar 100 µm.

eNeuro Accepted Manuscript

559 **References**

560 Ables JL, Görlich A, Antolin-Fontes B, Wang C, Lipford SM, Riad MH, Ren J, Hu F, Luo M, Kenny
561 PJ, Heintz N, Ibañez-Tallon I (2017) Retrograde inhibition by a specific subset of interpeduncular
562 α5 nicotinic neurons regulates nicotine preference. Proc Natl Acad Sci U S A 114:13012–13017.
563 Adell A, Artigas F (2004) The somatodendritic release of dopamine in the ventral tegmental area and its
564 regulation by afferent transmitter systems. Neuroscience & Biobehavioral Reviews 28:415–431.
565 Antolin-Fontes B, Ables JL, Görlich A, Ibañez-Tallon I (2015) The habenulo-interpeduncular pathway
566 in nicotine aversion and withdrawal. Neuropharmacology.
567 Aransay A, Rodríguez-López C, García-Amado M, Clascá F, Prensa L (2015) Long-range projection
568 neurons of the mouse ventral tegmental area: A single-cell axon tracing analysis. Frontiers in
569 Neuroanatomy 9:59.
570 Arber S, Costa RM (2022) Networking brainstem and basal ganglia circuits for movement. Nature
571 Reviews Neuroscience 2022 23:6 23:342–360.
572 Bäckman CM, Malik N, Zhang YJ, Shan L, Grinberg A, Hoffer BJ, Westphal H, Tomac AC (2006)
573 Characterization of a mouse strain expressing Cre recombinase from the 3' untranslated region of
574 the dopamine transporter locus. Genesis 44:383–390.
575 Bariselli S, Hörnberg H, Prévost-Solié C, Musardo S, Hatstatt-Burklé L, Scheiffele P, Bellone C (2018)
576 Role of VTA dopamine neurons and neuroligin 3 in sociability traits related to nonfamiliar
577 conspecific interaction. Nature Communications.
578 Beier KT, Steinberg EE, Deloach KE, Xie S, Miyamichi K, Schwarz L, Gao XJ, Kremer EJ, Malenka
579 RC, Luo L (2015) Circuit Architecture of VTA Dopamine Neurons Revealed by Systematic Input-
580 Output Mapping. Cell 162:622–634.
581 Berke JD (2018) What does dopamine mean? Nature Neuroscience.
582 Berrettini W, Yuan X, Tozzi F, Song K, Francks C, Chilcoat H, Waterworth D, Muglia P, Mooser V
583 (2008) α-5/α-3 nicotinic receptor subunit alleles increase risk for heavy smoking. Molecular
584 Psychiatry 2008 13:4 13:368–373.
585 Berridge KC, Robinson TE (1998) What is the role of dopamine in reward: Hedonic impact, reward
586 learning, or incentive salience? Brain Research Reviews.
587 Bierut LJ et al. (2008) Variants in nicotinic receptors and risk for nicotine dependence. American
588 Journal of Psychiatry 165:1163–1171.
589 Broussard GJ, Liang Y, Fridman M, Unger EK, Meng G, Xiao X, Ji N, Petreanu L, Tian L (2018) In
590 vivo measurement of afferent activity with axon-specific calcium imaging. Nature Neuroscience
591 2018 21:9 21:1272–1280.
592 Casserly AP, Tsuji J, Zhao-Shea R, Smith CB, Molas S, Tapper AR, Weng Z, Gardner PD (2020)
593 Integrated miRNA-/mRNA-Seq of the Habenulo-Interpeduncular Circuit During Acute Nicotine
594 Withdrawal. Scientific Reports 2020 10:1 10:1–14.
595 Chevallier C, Kohls G, Troiani V, Brodkin ES, Schultz RT (2012) The social motivation theory of
596 autism. Trends Cogn Sci 16:231–239.
597 Dalgleish HWP, Russell LE, Packer AM, Roth A, Gauld OM, Greenstreet F, Thompson EJ, Häusser M
598 (2020) How many neurons are sufficient for perception of cortical activity? Elife 9:1–99.
599 de Jong JW, Afjei SA, Pollak Dorocic I, Peck JR, Liu C, Kim CK, Tian L, Deisseroth K, Lammel S
600 (2019) A Neural Circuit Mechanism for Encoding Aversive Stimuli in the Mesolimbic Dopamine
601 System. Neuron.
602 DeGroot SR, Zhao-Shea R, Chung L, Klenowski PM, Sun F, Molas S, Gardner PD, Li Y, Tapper AR
603 (2020) Midbrain Dopamine Controls Anxiety-like Behavior by Engaging Unique Interpeduncular
604 Nucleus Microcircuitry. Biological Psychiatry.

eNeuro Accepted Manuscript

eNeuro Accepted Manuscript

605 Ferreira JGP, Del-Fava F, Hasue RH, Shammah-Lagnado SJ (2008) Organization of ventral tegmental
606 area projections to the ventral tegmental area–nigral complex in the rat. Neuroscience 153:196–
607 213.
608 Flagel SB, Clark JJ, Robinson TE, Mayo L, Czuj A, Willuhn I, Akers CA, Clinton SM, Phillips PEM,
609 Akil H (2010) A selective role for dopamine in stimulus–reward learning. Nature 2010 469:7328
610 469:53–57.
611 Floresco SB (2015) The Nucleus Accumbens: An Interface Between Cognition, Emotion, and Action.
612 http://dx.doi.org/101146/annurev-psych-010213-115159 66:25–32.
613 Fowler CD, Lu Q, Johnson PM, Marks MJ, Kenny PJ (2011) Habenular α5 nicotinic receptor subunit
614 signalling controls nicotine intake. Nature.
615 Frahm S, Ślimak MA, Ferrarese L, Santos-Torres J, Antolin-Fontes B, Auer S, Filkin S, Pons S,
616 Fontaine JF, Tsetlin V, Maskos U, Ibañez-Tallon I (2011) Aversion to Nicotine Is Regulated by the
617 Balanced Activity of β4 and α5 Nicotinic Receptor Subunits in the Medial Habenula. Neuron.
618 Görlich A, Antolin-Fontes B, Ables JL, Frahm S, Ślimak MA, Dougherty JD, Ibañez-Tallon I (2013)
619 Reexposure to nicotine during withdrawal increases the pacemaking activity of cholinergic
620 habenular neurons. Proc Natl Acad Sci U S A.
621 Groenewegen HJ, Ahlenius S, Haber SN, Kowall NW, Nauta WJH (1986) Cytoarchitecture, fiber
622 connections, and some histochemical aspects of the interpeduncular nucleus in the rat. Journal of
623 Comparative Neurology 249:65–102.
624 Gunaydin LA, Grosenick L, Finkelstein JC, Kauvar I v., Fenno LE, Adhikari A, Lammel S, Mirzabekov
625 JJ, Airan RD, Zalocusky KA, Tye KM, Anikeeva P, Malenka RC, Deisseroth K (2014) Natural
626 neural projection dynamics underlying social behavior. Cell.
627 Hemmendinger LM, Moore RY (1984) Interpeduncular nucleus organization in the rat: Cytoarchitecture
628 and histochemical analysis. Brain Research Bulletin.
629 Heymann G, Jo YS, Reichard KL, McFarland N, Chavkin C, Palmiter RD, Soden ME, Zweifel LS
630 (2020) Synergy of Distinct Dopamine Projection Populations in Behavioral Reinforcement. Neuron
631 105:909-920.e5.
632 Horga G, Abi-Dargham A (2019) An integrative framework for perceptual disturbances in psychosis.
633 Nature Reviews Neuroscience 2019 20:12 20:763–778.
634 Hung LW, Neuner S, Polepalli JS, Beier KT, Wright M, Walsh JJ, Lewis EM, Luo L, Deisseroth K,
635 Dölen G, Malenka RC (2017) Gating of social reward by oxytocin in the ventral tegmental area.
636 Science (1979).
637 Improgo MRD, Scofield MD, Tapper AR, Gardner PD (2010) The nicotinic acetylcholine receptor
638 CHRNA5/A3/B4 gene cluster: Dual role in nicotine addiction and lung cancer. Progress in
639 Neurobiology 92:212–226.
640 Klenowski PM, Zhao-Shea R, Freels TG, Molas S, Tapper AR (2021) Dynamic activity of
641 interpeduncular nucleus GABAergic neurons controls expression of nicotine withdrawal in male
642 mice. Neuropsychopharmacology 2021 47:3 47:641–651.
643 Kutlu MG, Zachry JE, Melugin PR, Cajigas SA, Chevee MF, Kelly SJ, Kutlu B, Tian L, Siciliano CA,
644 Calipari ES (2021) Dopamine release in the nucleus accumbens core signals perceived saliency.
645 Curr Biol 31:4748-4761.e8.
646 Lammel S, Hetzel A, Häckel O, Jones I, Liss B, Roeper J (2008) Unique Properties of Mesoprefrontal
647 Neurons within a Dual Mesocorticolimbic Dopamine System. Neuron.
648 Lammel S, Ion DI, Roeper J, Malenka RC (2011) Projection-Specific Modulation of Dopamine Neuron
649 Synapses by Aversive and Rewarding Stimuli. Neuron.
650 Lammel S, Lim BK, Malenka RC (2014) Reward and aversion in a heterogeneous midbrain dopamine
651 system. Neuropharmacology 76:351–359.

eNeuro Accepted Manuscript

652 Lammel S, Lim BK, Ran C, Huang KW, Betley MJ, Tye KM, Deisseroth K, Malenka RC (2012) Input-
653 specific control of reward and aversion in the ventral tegmental area. Nature.
654 Lammel S, Steinberg EE, Földy C, Wall NR, Beier K, Luo L, Malenka RC (2015) Diversity of
655 Transgenic Mouse Models for Selective Targeting of Midbrain Dopamine Neurons. Neuron
656 85:429–438.
657 Lima LB, Bueno D, Leite F, Souza S, Gonçalves L, Furigo IC, Donato J, Metzger M (2017) Afferent
658 and efferent connections of the interpeduncular nucleus with special reference to circuits involving
659 the habenula and raphe nuclei. Journal of Comparative Neurology 525:2411–2442.
660 Marshel JH, Kim YS, Machado TA, Quirin S, Benson B, Kadmon J, Raja C, Chibukhchyan A,
661 Ramakrishnan C, Inoue M, Shane JC, McKnight DJ, Yoshizawa S, Kato HE, Ganguli S, Deisseroth
662 K (2019) Cortical layer-specific critical dynamics triggering perception. Science (1979) 365.
663 Matsumoto M, Hikosaka O (2009) Two types of dopamine neuron distinctly convey positive and
664 negative motivational signals. Nature.
665 Mirenowicz J, Schultz W (1996) Preferential activation of midbrain dopamine neurons by appetitive
666 rather than aversive stimuli. Nature 1996 379:6564 379:449–451.
667 Molas S, DeGroot SR, Zhao-Shea R, Tapper AR (2017a) Anxiety and Nicotine Dependence: Emerging
668 Role of the Habenulo-Interpeduncular Axis. Trends in Pharmacological Sciences 38.
669 Molas S, Zhao-Shea R, Liu L, Degroot SR, Gardner PD, Tapper AR (2017b) A circuit-based mechanism
670 underlying familiarity signaling and the preference for novelty. Nature Neuroscience 20.
671 Morales M, Margolis EB (2017) Ventral tegmental area: cellular heterogeneity, connectivity and
672 behaviour. Nature Reviews Neuroscience 2017 18:2 18:73–85.
673 Nasirova N, Quina LA, Novik S, Turner EE (2021) Genetically Targeted Connectivity Tracing Excludes
674 Dopaminergic Inputs to the Interpeduncular Nucleus from the Ventral Tegmentum and Substantia
675 Nigra. eNeuro 8.
676 Nestler EJ, Lüscher C (2019) The Molecular Basis of Drug Addiction: Linking Epigenetic to Synaptic
677 and Circuit Mechanisms. Neuron 102:48–59.
678 Okuyama T, Kitamura T, Roy DS, Itohara S, Tonegawa S (2016) Ventral CA1 neurons store social
679 memory. Science (1979).
680 Patriarchi T, Cho JR, Merten K, Howe MW, Marley A, Xiong WH, Folk RW, Broussard GJ, Liang R,
681 Jang MJ, Zhong H, Dombeck D, von Zastrow M, Nimmerjahn A, Gradinaru V, Williams JT, Tian
682 L (2018) Ultrafast neuronal imaging of dopamine dynamics with designed genetically encoded
683 sensors. Science 360.
684 Paxinos G, Franklin KBJ (2001) The mouse brain in stereotaxic coordinates: hard cover edition.
685 Academic Press 2nd Editio:360.
686 Phillips RA, Tuscher JJ, Black SL, Andraka E, Fitzgerald ND, Ianov L, Day JJ (2022) An atlas of
687 transcriptionally defined cell populations in the rat ventral tegmental area. Cell Reports 39:110616.
688 Phillipson OT, Pycock CJ (1982) Dopamine neurones of the ventral tegmentum project to both medial
689 and lateral habenula. Experimental Brain Research 1982 45:1 45:89–94.
690 Poulin JF, Caronia G, Hofer C, Cui Q, Helm B, Ramakrishnan C, Chan CS, Dombeck DA, Deisseroth
691 K, Awatramani R (2018) Mapping projections of molecularly defined dopamine neuron subtypes
692 using intersectional genetic approaches. Nature Neuroscience 2018 21:9 21:1260–1271.
693 Poulin JF, Gaertner Z, Moreno-Ramos OA, Awatramani R (2020) Classification of midbrain dopamine
694 neurons using single-cell gene expression profiling approaches. Trends Neurosci 43:155.
695 Powell JM, Plummer NM, Scappini EL, Tucker CJ, Jensen P (2019) DEFiNE: A method for
696 enhancement and quantification of fluorescently labeled axons. Front Neuroanat 2019 12:117
697 Quina LA, Harris J, Zeng H, Turner EE (2017) Specific connections of the interpeduncular subnuclei
698 reveal distinct components of the habenulopeduncular pathway. Journal of Comparative Neurology.

eNeuro Accepted Manuscript

699 Ruitenberg MFL, van Wouwe NC, Wylie SA, Abrahamse EL (2021) The role of dopamine in action
700 control: Insights from medication effects in Parkinson's disease. Neuroscience & Biobehavioral
701 Reviews 127:158–170.
702 Salas R, Sturm R, Boulter J, de Biasi M (2009) Nicotinic Receptors in the Habenulo-Interpeduncular
703 System Are Necessary for Nicotine Withdrawal in Mice. Journal of Neuroscience 29:3014–3018.
704 Saunders BT, Richard JM, Margolis EB, Janak PH (2018) Dopamine neurons create Pavlovian
705 conditioned stimuli with circuit-defined motivational properties. Nat Neurosci 21:1072–1083.
706 Schultz W, Dayan P, Montague PR (1997) A neural substrate of prediction and reward. Science (1979).
707 Seigneur E, Polepalli JS, Südhof TC (2018) Cbln2 and Cbln4 are expressed in distinct medial habenula-
708 interpeduncular projections and contribute to different behavioral outputs. Proc Natl Acad Sci U S
709 A 115:E10235–E10244.
710 Sherafat Y, Bautista M, Fowler JP, Chen E, Ahmed A, Fowler CD (2020) The Interpeduncular-Ventral
711 Hippocampus Pathway Mediates Active Stress Coping and Natural Reward. eNeuro 7:1–17.
712 Solié C, Girard B, Righetti B, Tapparel M, Bellone C (2021) VTA dopamine neuron activity encodes
713 social interaction and promotes reinforcement learning through social prediction error. Nature
714 Neuroscience 2021 25:1 25:86–97.
715 Soria-Gómez E, Busquets-Garcia A, Hu F, Mehidi A, Cannich A, Roux L, Louit I, Alonso L, Wiesner T,
716 Georges F, Verrier D, Vincent P, Ferreira G, Luo M, Marsicano G (2015) Habenular CB1
717 Receptors Control the Expression of Aversive Memories. Neuron.
718 Swanson LW (1982) The projections of the ventral tegmental area and adjacent regions: A combined
719 fluorescent retrograde tracer and immunofluorescence study in the rat. Brain Research Bulletin
720 9:321–353.
721 Taylor WD, Zald DH, Felger JC, Christman S, Claassen DO, Horga G, Miller JM, Gifford K, Rogers B,
722 Szymkowicz SM, Rutherford BR (2021) Influences of dopaminergic system dysfunction on late-
723 life depression. Molecular Psychiatry 2021 27:1 27:180–191.
724 Tiklová K, Björklund ÅK, Lahti L, Fiorenzano A, Nolbrant S, Gillberg L, Volakakis N, Yokota C,
725 Hilscher MM, Hauling T, Holmström F, Joodmardi E, Nilsson M, Parmar M, Perlmann T (2019)
726 Single-cell RNA sequencing reveals midbrain dopamine neuron diversity emerging during mouse
727 brain development. Nature Communications 2019 10:1 10:1–12.
728 Walf AA, Frye CA (2007) The use of the elevated plus maze as an assay of anxiety-related behavior in
729 rodents. Nature Protocols 2007 2:2 2:322–328.
730 Watabe-Uchida M, Zhu L, Ogawa SK, Vamanrao A, Uchida N (2012) Whole-Brain Mapping of Direct
731 Inputs to Midbrain Dopamine Neurons. Neuron 74:858–873.
732 Wills L, Ables JL, Braunscheidel KM, Caligiuri SPB, Elayouby KS, Fillinger C, Ishikawa M, Moen JK,
733 Kenny PJ (2022) Neurobiological Mechanisms of Nicotine Reward and Aversion.
734 Yamaguchi T, Danjo T, Pastan I, Hikida T, Nakanishi S (2013) Distinct roles of segregated transmission
735 of the septo-habenular pathway in anxiety and fear. Neuron 78:537–544.
736 Zalachoras I, Astori S, Meijer M, Grosse J, Zanoletti O, de Suduiraut IG, Deussing JM, Sandi C (2022)
737 Opposite effects of stress on effortful motivation in high and low anxiety are mediated by CRHR1
738 in the VTA. Science Advances 8:SPOTLIGHTS.
739 Zhang J, Tan L, Ren Y, Liang J, Lin R, Feng Q, Zhou J, Hu F, Ren J, Wei C, Yu T, Zhuang Y, Bettler
740 B, Wang F, Luo M (2016) Presynaptic Excitation via GABAB Receptors in Habenula Cholinergic
741 Neurons Regulates Fear Memory Expression. Cell.
742 Zhang S, Xu M, Chang WC, Ma C, Hoang Do JP, Jeong D, Lei T, Fan JL, Dan Y (2016) Organization
743 of long-range inputs and outputs of frontal cortex for top-down control. Nature Neuroscience 2016
744 19:12 19:1733–1742.
745 Zhao-Shea R, Degroot SR, Liu L, Vallaster M, Pang X, Su Q, Gao G, Rando OJ, Martin GE, George O,
746 Gardner PD, Tapper AR (2015) Increased CRF signalling in a ventral tegmental area-

eNeuro Accepted Manuscript

747 interpeduncular nucleus-medial habenula circuit induces anxiety during nicotine withdrawal.
748 Nature Communications 2015 6:1 6:1–14.
749 Zhao-Shea R, Liu L, Pang X, Gardner PD, Tapper AR (2013) Activation of GABAergic Neurons in the
750 Interpeduncular Nucleus Triggers Physical Nicotine Withdrawal Symptoms. Current Biology
751 23:2327–2335.
752 Zweifel LS, Fadok JP, Argilli E, Garelick MG, Jones GL, Dickerson TMK, Allen JM, Mizumori SJY,
753 Bonci A, Palmiter RD (2011) Activation of dopamine neurons is critical for aversive conditioning
754 and prevention of generalized anxiety. Nature Neuroscience 2011 14:5 14:620–626.
755

eNeuro Accepted Manuscript

1

Table 1					
Figure	**Data structure**	**Type of test**	**value**	**Significance**	**95% confidence interval**
4B	normal distribution	unpaired two-tailed t-test	t(10) =4.546	p=0.0011	1005 to 2937
4D	normal distribution	unpaired two-tailed t-test	t(10) =3.438	p=0.0064	472.4 to 2213
4E	normal distribution	unpaired two-tailed t-test	t(10) =3.114	p=0.011	88.7 to 535
4F	normal distribution	unpaired two-tailed t-test	t(10) =0.184	p=0.8577	-1530 to 1297
5I	normal distribution	One-way repeated measures(RM) ANOVA	F(3,39)=21.8	p<0.0001	
		Dunnett's multiple comparisons test		-1-0 s vs. 1-2s p<0.001	-0.467 to -0.225
				-1-0 s vs. 2-3s p<0.01	-0.7073 to -0.2226
5L	normal distribution	One-way repeated measures(RM) ANOVA	F(3,39)=0.7103	p=0.517	
5O	normal distribution	two-way repeated measures(RM) ANOVA	interaction F(1,29)=19.13	p=0.0001	-0.6159 to -0.1622
		Bonferroni multiple comparisons test		event signal vs.random p<0.0001	
5R	normal distribution	two-way repeated measures(RM) ANOVA	interaction F(1,26)=1.423	p=0.2436	
6E	normal distribution	One-way repeated measures(RM) ANOVA	F(3,67)=18.15	p<0.0001	
		Dunnett's multiple comparisons test		-1-0 vs. 0-1 p=0.0007	-0.4559 to -0.1324
				-1-0 vs. 1-2 p=0.0042	-0.6817 to -0.1301
				-1-0 vs. 2-3 p=0.0001	-0.958 to -0.3466
6H	normal distribution	One-way repeated measures(RM) ANOVA	F(3,67)=7.617	p=0.0042	
		Dunnett's multiple comparisons test		-1-0 vs. 0-1 p=0.0005	0.1783 to 0.5891
				-1-0 vs. 1-2 p=0.0152	0.0677 to 0.6580
				-1-0 vs. 2-3 p=0.032	0.029 to 0.6929
6K	normal distribution	two-way repeated measures(RM) ANOVA	interaction F(2,36)=4.136	p=0.0242	-0.54 to 0.2074
		Bonferroni multiple comparisons test		signal open vs. close p=0.0008	
				signal open vs. random p=0.0047	

2

eNeuro Accepted Manuscript

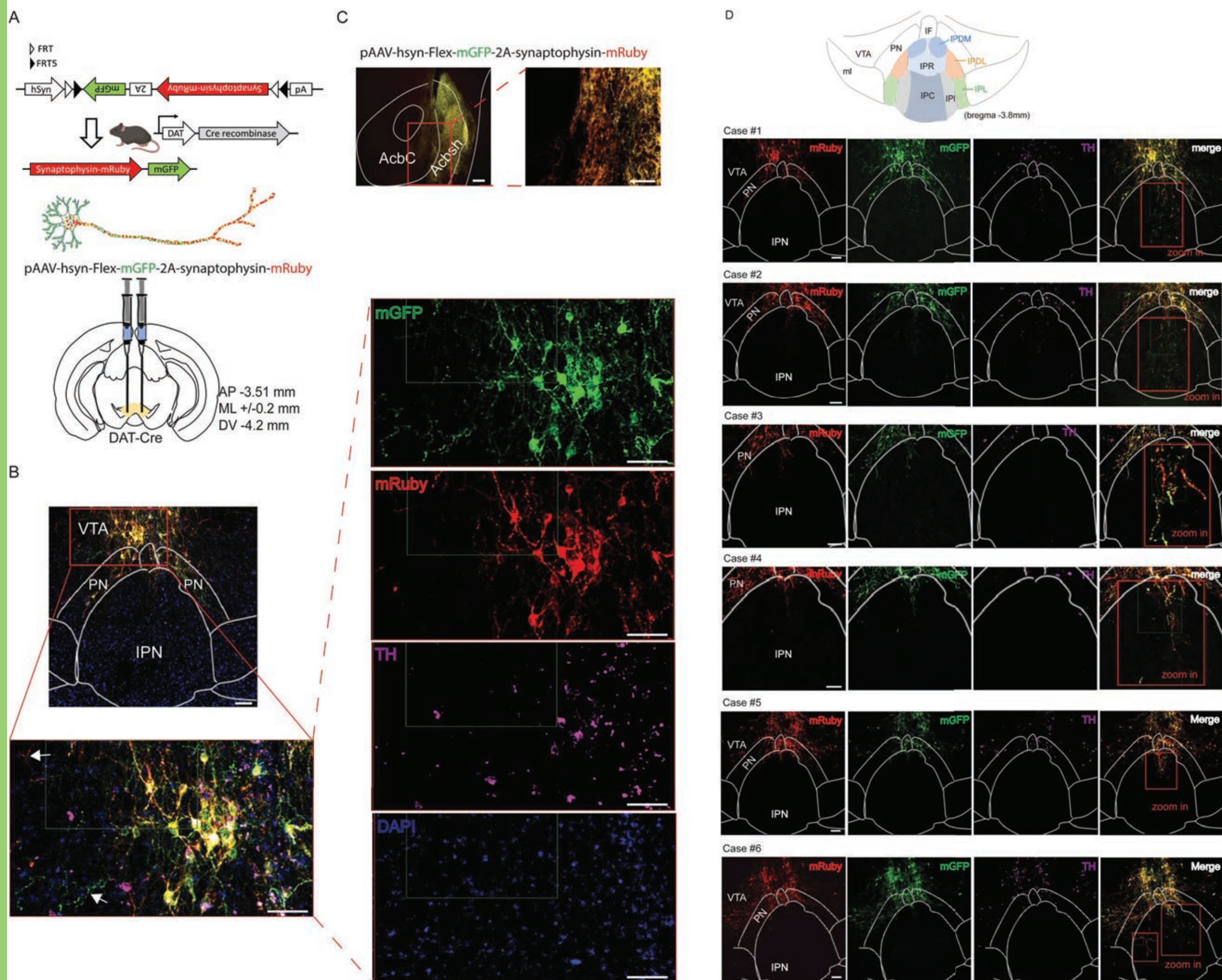

eNeuro Accepted Manuscript

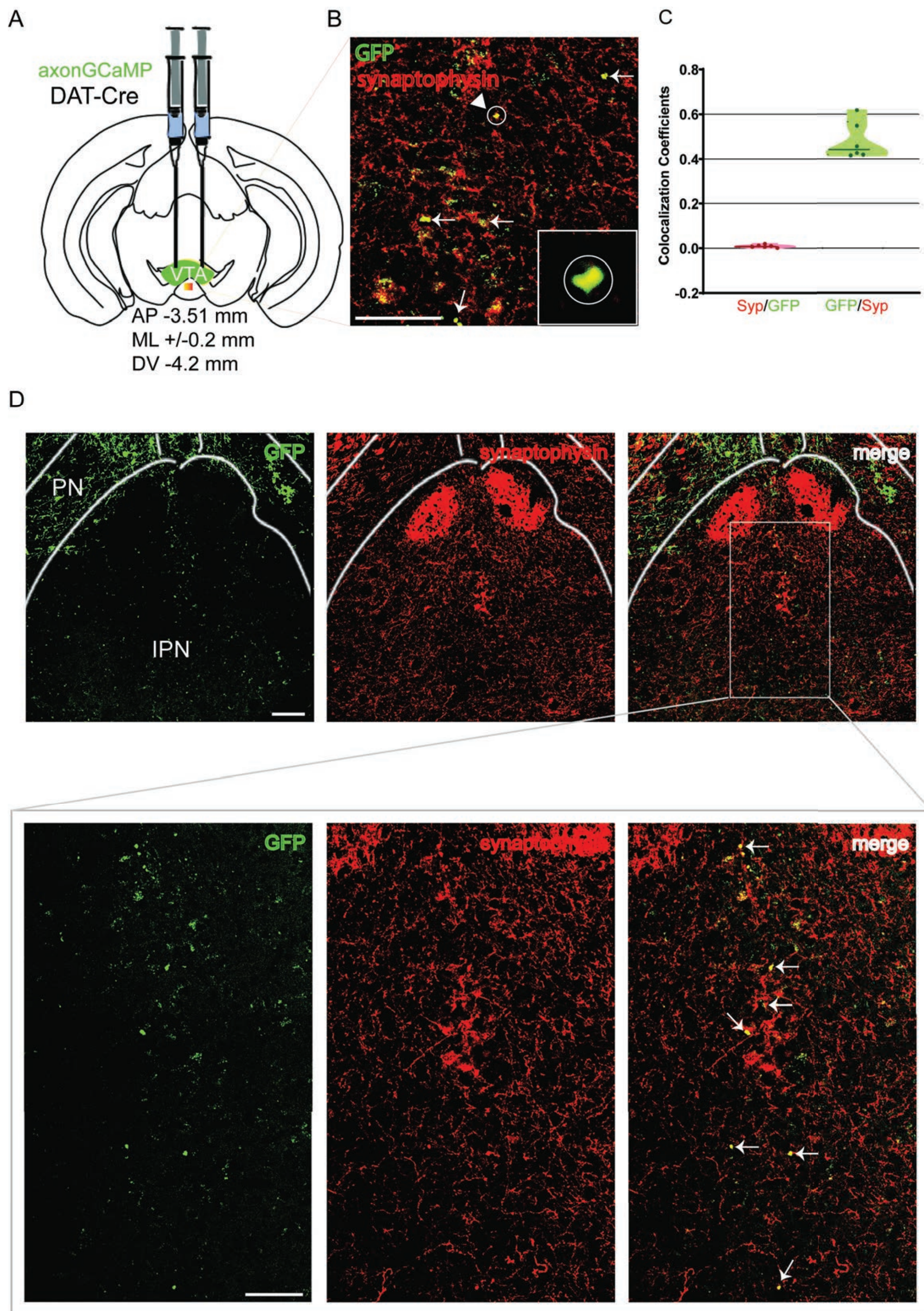

eNeuro Accepted Manuscript

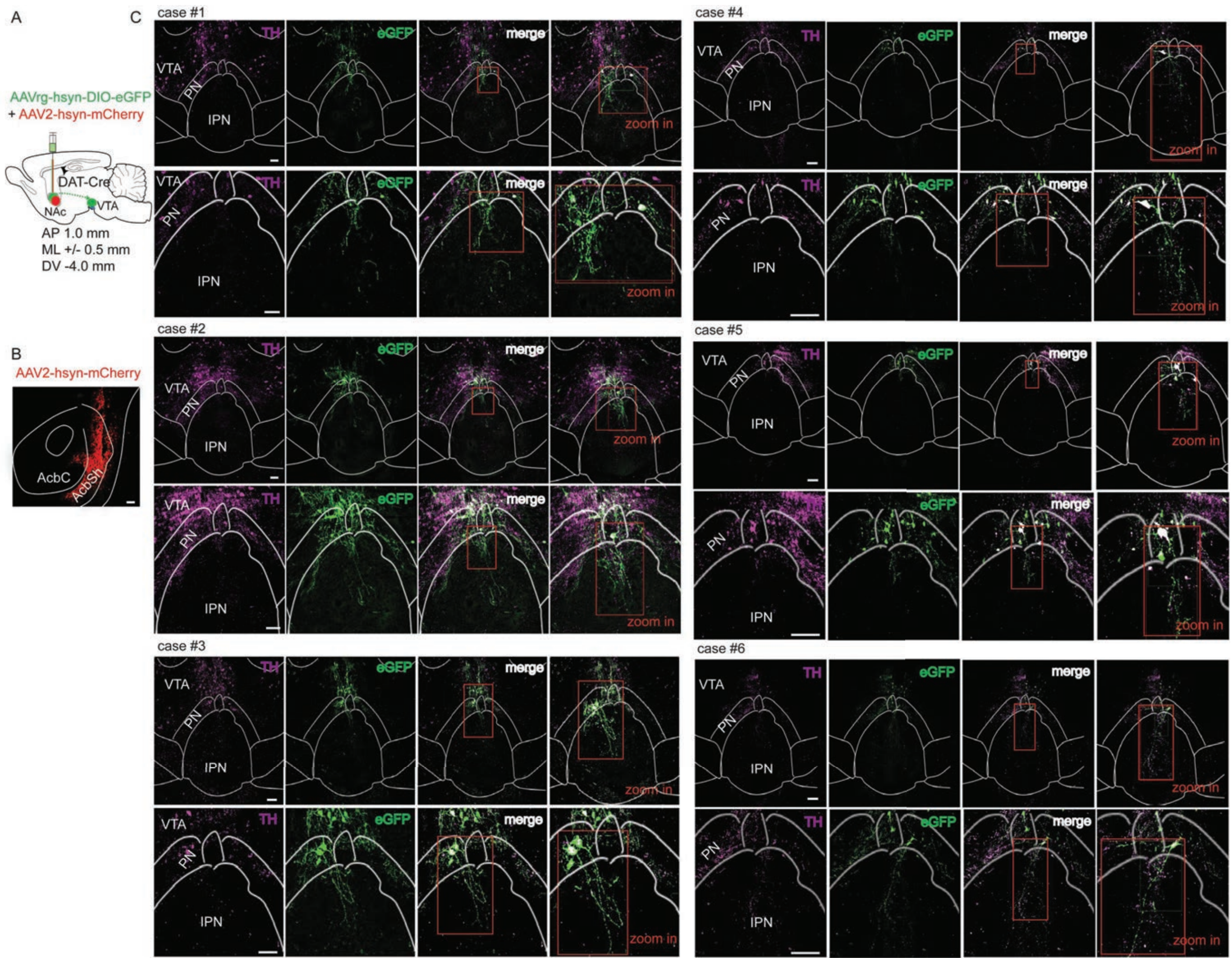

eNeuro Accepted Manuscript

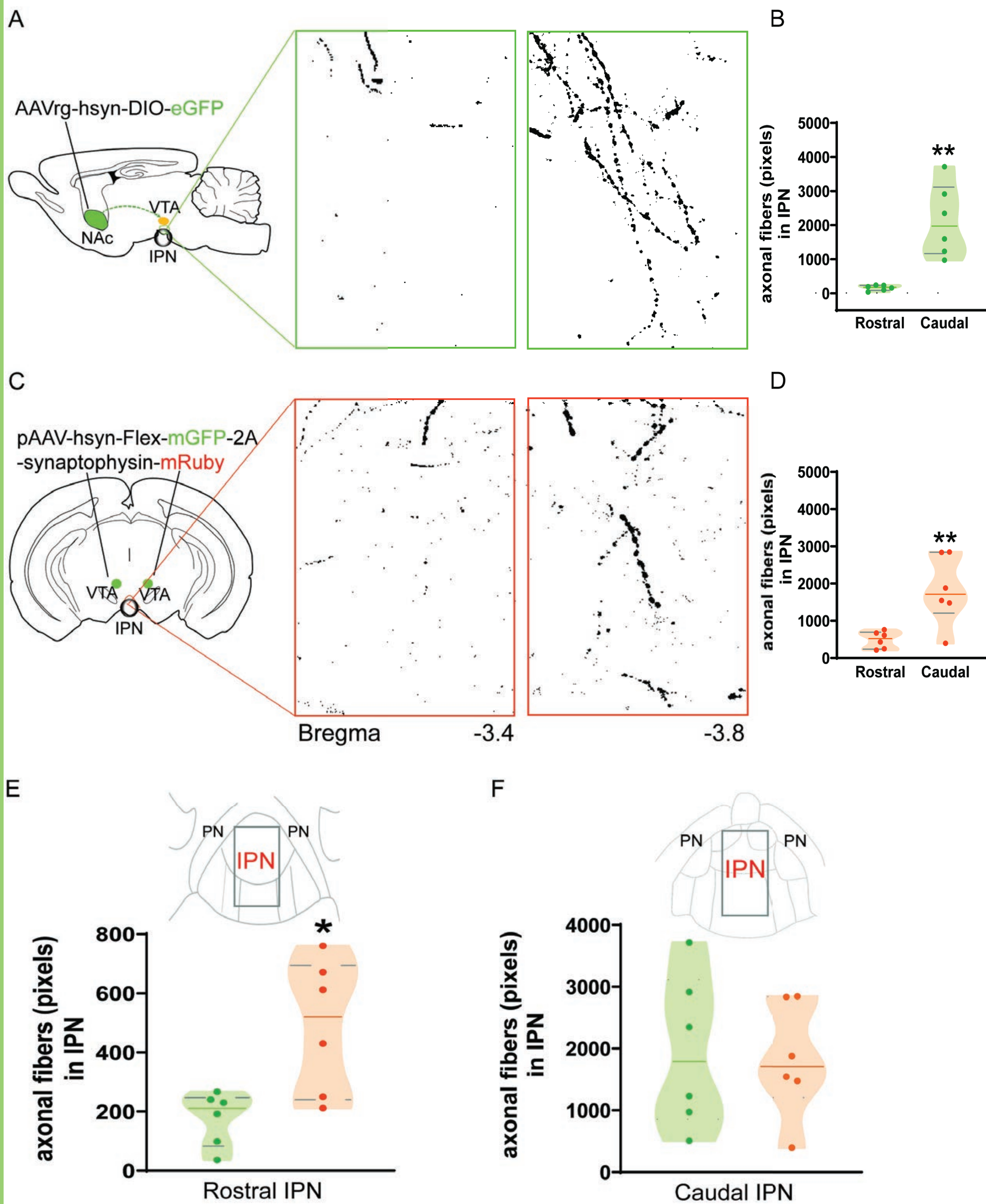

eNeuro Accepted Manuscript

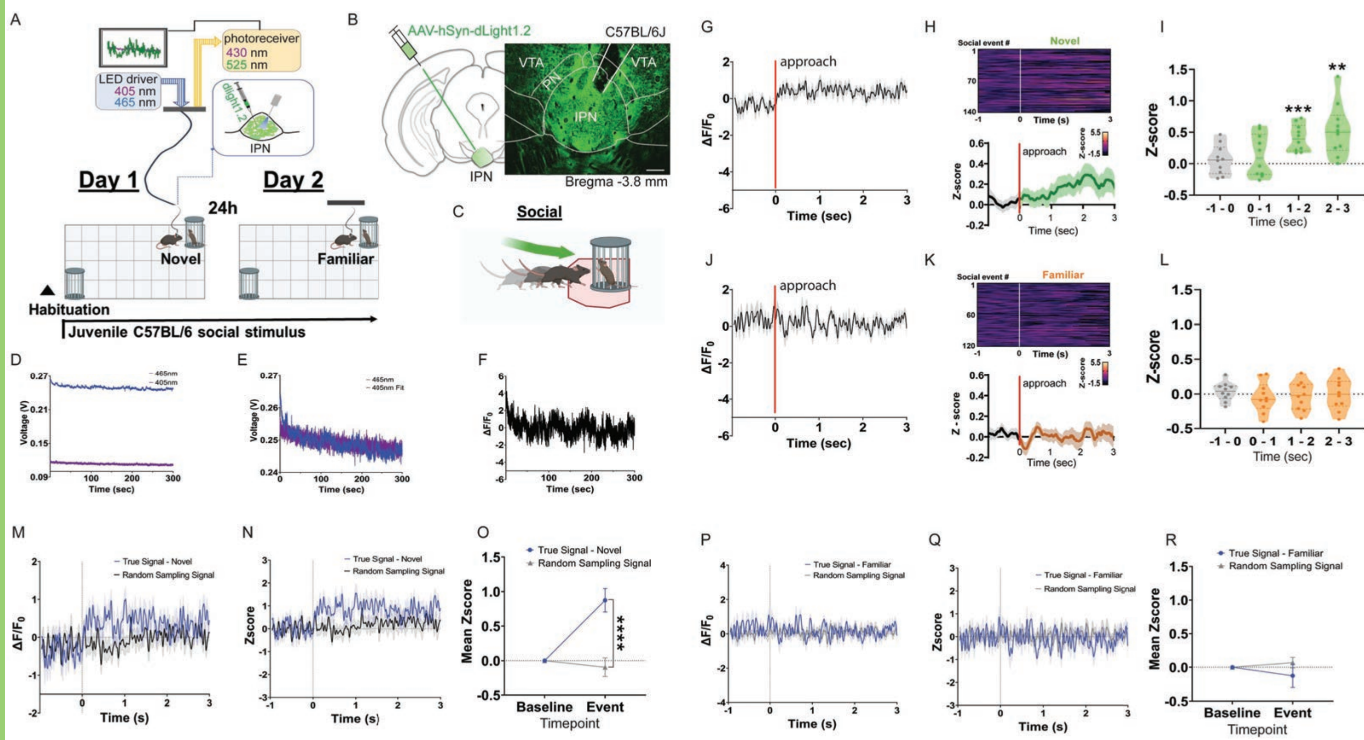

eNeuro Accepted Manuscript

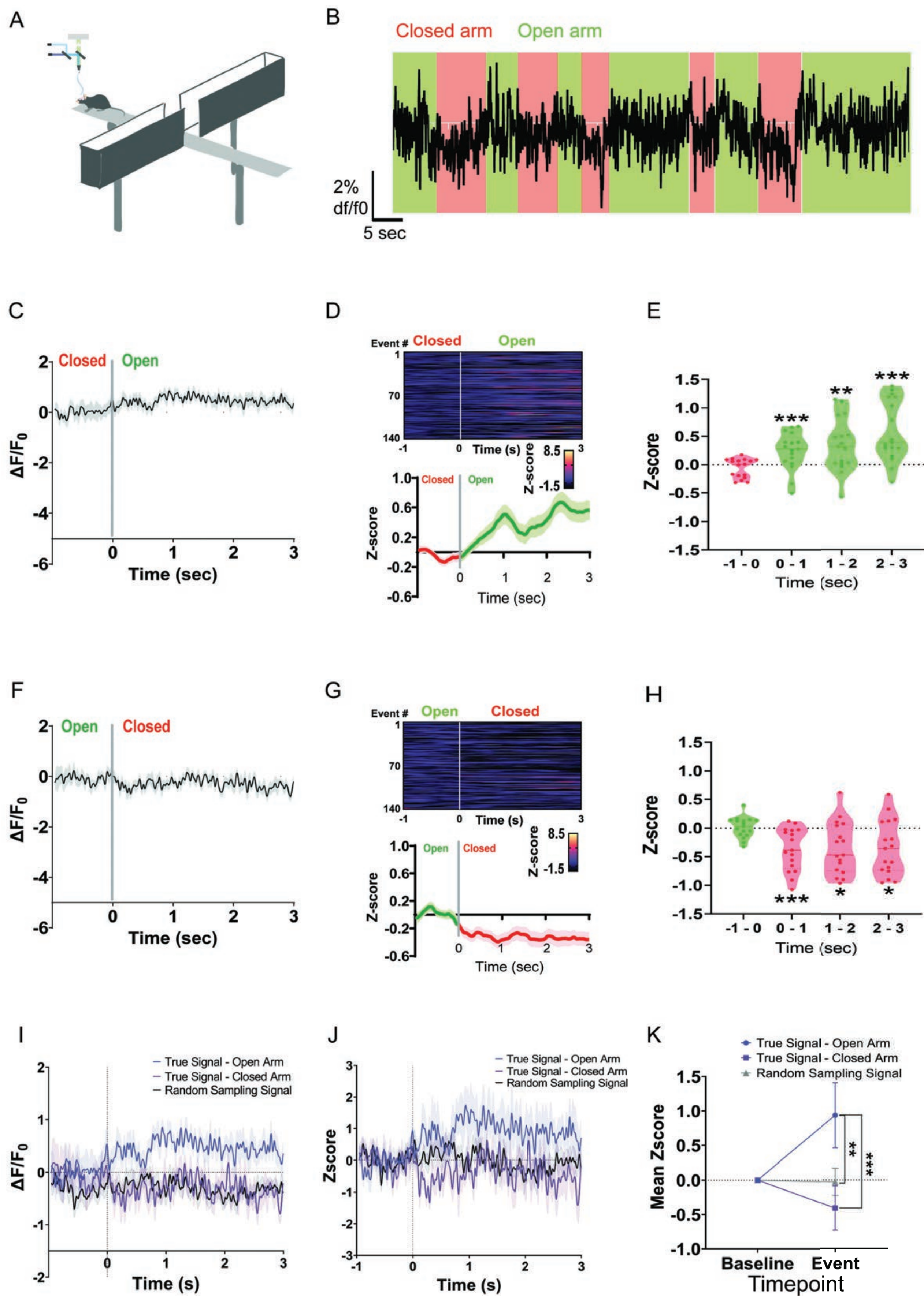

eNeuro Accepted Manuscript